Empirical Characterization of Lateral Crosstalk for CMOS Image Sensors and Deblurring Operations

J. S. Lee, J. Shah[1], M. Ed Jernigan[2], and R. I. Hornsey[3]
Dept. of Electrical and Computer Engineering, University of Waterloo, Ontario, Canada
[1]Micron Imaging, Boise, Idaho
[2]Dept. of Systems Design Engineering, University of Waterloo, Ontario, Canada
[3]Dept. of Computer Science (and Dept. of Physics), York University, Ontario, Canada
hornsey@cs.yorku.ca, Tel: (416) 736-2100 ext.33265, FAX: (416) 736-5872

Abstract—**Lateral crosstalk in CMOS imaging arrays deter effective utilization of small pixel sizes (e.g. < 5.0 μm x 5.0 μm) now permitted by technology scaling. A simple measurement setup for empirical characterization of lateral crosstalk in CMOS image sensors is presented. A demonstration of deblurring operations based on the obtained blur model of lateral crosstalk is also provided. Several well-known linear deconvolution filters are employed in the demonstration. The tradeoffs in sharpness restoration, high-frequency noise amplification, and the intensity clipping effect in the design of linear deblurring operation for the application of lateral crosstalk are illustrated.**

I. Introduction

We present an alternative method for empirical characterization of lateral crosstalk with a demonstration of cross-responsivity PSF measurement using a laser spot illumination. A number of studies have already reported utilizing laser scanning technique to characterize sub-pixel and lateral photoresponse in CMOS imaging arrays [1]–[4]. In this work, we illustrate a much simpler setup that is generally sufficient for measuring cross-responsivity PSF. A comparative look at the results of the employed linear deconvolution filters illustrates several of the important trade-offs in devising an appropriate deblurring operation for lateral crosstalk in CMOS image sensors.

Consider a linear model of a CMOS image sensor depicted in Fig. 1. H_{optics} represent the effects of optics, which may involve one or more lenses, anti-reflection coating(s), micro-lenses, and dielectric layers [5]–[7]. $H_{\text{diffusion}}$ represents to the blurring effects of lateral diffusion [8]–[26]. $H_{\text{integration}}$ represents the spatial (and temporal) integration of photocarriers along the area of the photosensitive device in each pixel [27]. H_{sampling} represents to the spatial discretization of the continuous image (i.e. multiplication with an impulse train). Assuming a square pixel with pitch, p, the spatial Nyquist frequency in each dimension is $f_{\text{Nyquist}} = 1/2p$ and scenes with spatial frequencies greater than f_{Nyquist} cannot be reliably reproduced. H_{optics}, $H_{\text{diffusion}}$, and $H_{\text{integration}}$ each degrade the reproduction of frequencies below f_{Nyquist} by a low-pass filtering effect, which may be characterized as MTF_{optics}, $MTF_{\text{diffusion}}$, and $MTF_{\text{integration}}$, respectively [27]. As it is generally convenient to consider optical effects separately from the semiconductor phenomena, the internal cross-responsivity of an imaging array is defined as

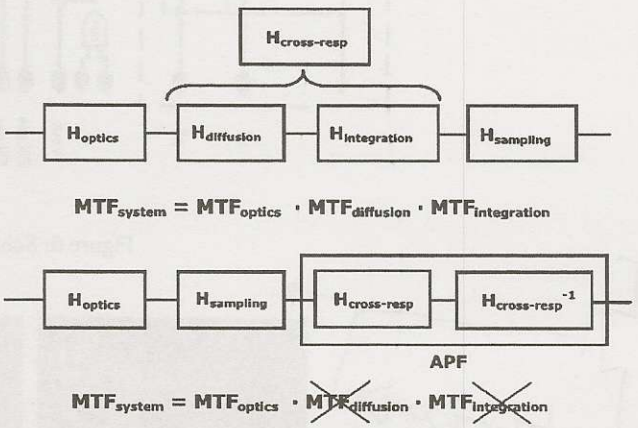

Fig. 1 Simple linear model of CMOS image sensor.

$$H_{\text{cross-responsivity}}(f) = H_{\text{diffusion}}(f) \cdot H_{\text{integration}}(f) \quad \text{for } f < f_{\text{Nyquist}} \quad (1)$$

Fig. 2 illustrates the measurement setup for an empirical characterization of internal cross-responsivity of an image sensor. A Ne-He laser (λ = 633 nm) coupled to a thin core optical fiber (4.0 μm) with a pigtail style fiber focuser was employed for the experiment. The laser beam is focused onto a single pixel area and the generated photocarriers diffuse in all direction. The collection outcome of the photocarrier diffusion can be extracted from the sensor output. For sake of simplicity, we assume the measurement can be taken in the linear region of sensor operation with a proper selection of the integration time and the intensity of the illumination spot.

With the raster spot-scanning technique [1]–[3], only the scanning field needs to be adjusted to accommodate different pixel sizes and shapes. Yet, the single spot illumination requires a much simpler setup and can be easily repeated on different pixels for a verification of measurement consistency. The circular shape of the spot, however, prevents the full coverage of corner areas of a square pixel. The corner regions of a square pixel not enclosed by a circular spot (having an identical diameter as the pixel) represent 21.5% of the total area. While this represents a significant percentage of the total area, the peripheral regions of a pixel employing an active readout circuitry are generally occupied by metal interconnect lines, which significantly reduce the size of pixel area susceptible to illumination. Fig. 2 examines the dimensions of

the areas unenclosed by the circular spot for various pixel sizes. For rectangular pixels, the circular spot may leave a considerably larger area unenclosed, and hence a different technique such as laser spot-scanning may be necessary.

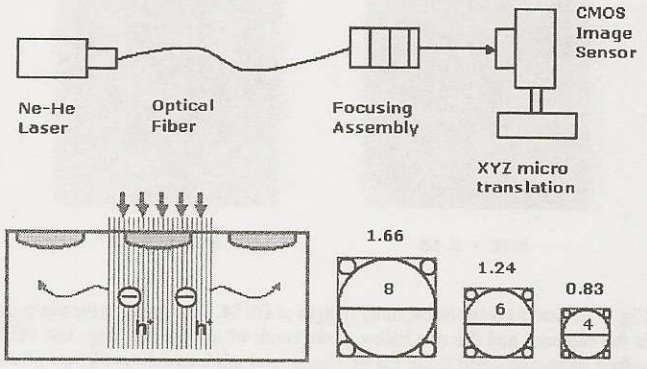

Fig. 2 The measurement setup for cross-responsivity PSF. Ne-He laser (l = 633 nm) is coupled to a thin core optical fiber (4.0 μm) with a pigtail style fiber focuser. The diameters of the corner circles are shown above each pixel diagram.

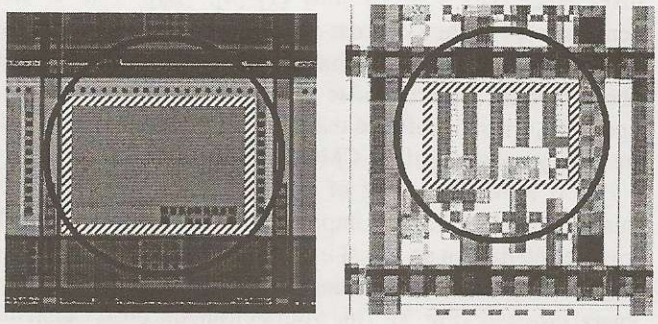

(a) (b)

Fig. 3 Examples of CMOS active pixel sensors layout. (a) 22 μm x 22 μm APS in a standard 0.35 μm CMOS technology and (b) 10 μm x 10 μm APS in a standard 0.50 μm CMOS technology. The rectangular outline (in diagonal stripes) marks the photodiode area in each pixel. Each circle (in solid dark line) illustrates the spot size whose diameter is identical to the side length of each pixel. The dark regions in each layout represent metal interconnects in the pixel.

Model	Technology	Pixel Pitch	Resolution	Fill Factor
IBIS4 (FillFactory)	n/a (VDD=5.0V)	7.0 ìm	1280x1024	60 %
ZR32112 (Zoran)	0.25 μm	7.5 ìm	1280x1024	51 %
ICDWTST4 (custom)	TSMC 0.35 μm	22 ìm	104x104	41 %
ICCWTCYC (custom)	HP 0.50 μm	30 ìm	64x64	60 %

Table 1 Some Information about the four CMOS image sensors in Fig. 4.

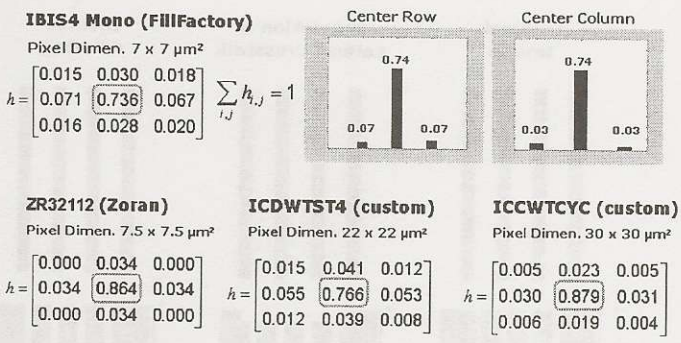

Fig. 4 Measured cross-responsivity PSF obtained from four CMOS image sensors. The measured cross-responsivity PSF are each scaled to provide a blur model with unity DC gain (i.e. $\Sigma a_{ij} = 1$).

The measured cross-responsivity PSFs are shown in Fig. 4. Table 1 provides some information about the four CMOS image sensors. The spot size was adjusted for each image sensor so that it is slightly smaller than the size of a single pixel, ensuring that the resulting lateral photoresponse is not based on an excitation of a small portion of the whole pixel area. This was accomplished by adjusting the working distance between the fiber focuser and CMOS image sensor manually with a micro-translator. A low integration time was employed to help distinguish spot over-sizing from the effects of lateral crosstalk. Upon adjusting the spot size, the integration time was also adjusted on each image sensor so that the illuminated pixel yielded 90% to 95% of the saturation output level. This was done to ensure a high signal-to-noise ratio while avoiding pixel blooming. An optical table was used to minimize the effects of vibration.

The measured cross-responsivity PSF were each scaled to provide a blur model with unity DC gain (i.e. $\Sigma a_{ij} = 1$). The percentage of photocarriers participating in lateral crosstalk can be inferred from the center value of the cross-responsivity PSF; for example, the center value of 73.6% for the commercial IBIS4 sensor indicates that 26.4% of the photocarriers excited from the center pixel manifest in the neighboring pixels. Examining the results of Fig. 3, it can be seen that the smaller pixels generally show higher lateral crosstalk as expected. An exception is found with ZR32112, which exhibits an anisotropic PSF with a relatively little lateral crosstalk.

Several fabrication process characteristics can significantly vary lateral photoresponse from one technology to another, including the epitaxial layer thickness [20], [26], the epitaxial and substrate doping [4], the surface recombination and mobility degradation near the $Si\text{-}SiO_2$ interface [26], as well as the optical characteristics of the technology [6], [27]. From Fig. 4, it is also evident that some cross-responsivity PSFs are slightly asymmetric. While bulk diffusion is practically isotropic for imaging applications, the presence of reverse biased junctions and gate electric fields in a pixel structure can significantly deter lateral diffusion. The asymmetry of lateral photoresponse in CMOS active pixel sensors were also

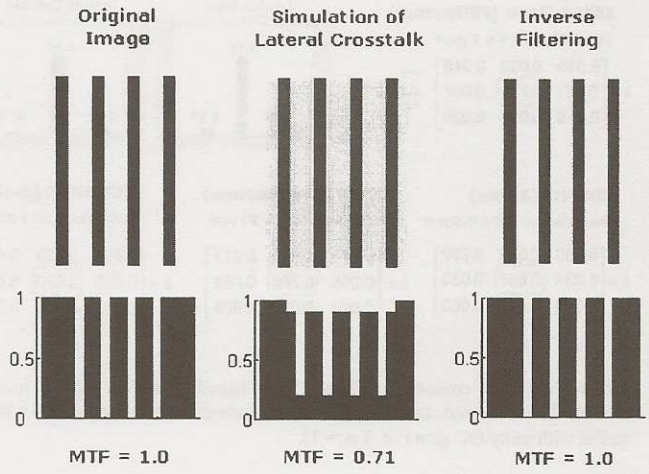

Fig. 5 A test image consisting of several black stripes on a white background convolved with the cross-responsivity PSF of IBIS4. The resulting loss of contrast characterized by MTF degradation is found to be about 29% – slightly higher than 26.4% indicated by the cross-responsivity PSF – as the photocarriers lost to lateral crosstalk manifest in the neighboring pixels to further degrade the contrast gradient.

demonstrated with the sub-pixel photoresponse characterizations performed with the spot-scanning technique [1]–[3].

The loss of photocarriers to lateral crosstalk directly translates to a loss of image contrast as illustrated in Fig. 5, which shows a test image consisting of several black stripes on a white background convolved with the cross-responsivity PSF of IBIS4. Fig. 5 also shows the result of applying the inverse filter on the blurred image, i.e.

$$G_{inverse} = H_{\text{cross-responsivity}}^{-1} \quad (2)$$

In the next section, we discuss the conditions necessary for an effective restoration of images from the blurring effects of lateral crosstalk. Several well-known linear deconvolution filters are also demonstrated, illustrating some of the tradeoffs in designing a linear deblurring operation for image sensor applications.

II. Comparison of Deblurring Filters

For exponential or Gaussian type blurring, the Fourier transform of the blur model shows a frequency response that is non-zero at all frequencies, implying that the blur process preserves all frequency components of the original image.[†] In practical imaging systems with finite range of operating frequencies, it can be generally stated that a blur process must preserve all significant frequency components of an image with respect to the system's minimum noise limit in order for the blur process to be effectively reversible. Several investigations

[†] A local average filter, on the other hand, has frequency response of the form sin(f)/f and demonstrates a non-invertible blur process [28].

of

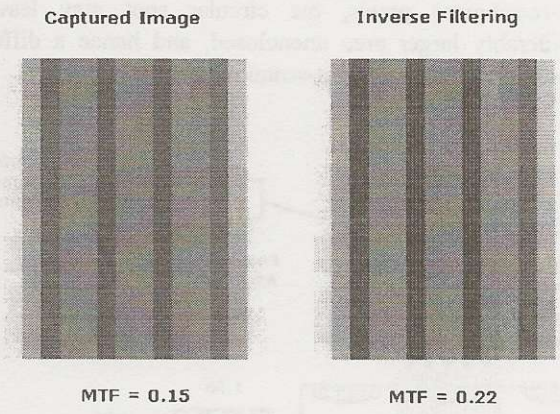

Fig. 1 Inverse filtering on captured images of IBIS4. The figure on the top-right is the captured and the one below is the result of inverse filtering. The MTF values were calculated using the maximum and minimum output levels of the image sensor.

lateral photoresponse in modern CMOS image sensors have revealed that the characteristic distance of spatial decay of lateral photoresponse is generally comparable to the typical pixel sizes (i.e. 5 ~ 10 μm) [1]–[4], [26]. This is also demonstrated by the 3x3 cross-responsivity PSFs shown in Fig. 3. From the observation that the spatial extent of lateral photoresponse is comparable to the period of the sampling operation, it can be inferred that $H_{\text{diffusion}}$ likely spans the whole frequency spectrum of the CMOS imaging array.

Fig. 6 shows the result of inverse filtering on a captured image from IBIS4. The improvement of contrast from the inverse filtering on an actual image output of IBIS4 in Fig. 6 is considerably smaller than the previous case with simulated lateral crosstalk (Fig. 5). This follows from the observation that the images captured by an image sensor undergo a number of other blurring processes in addition to the lateral crosstalk such as those arising from the image sensor optics (i.e. H_{optics}). Fig. 6 also shows that inverse filtering leads to a slight amplification of high-frequency noise (e.g. fixed pattern noise). It is useful to note an inverse filter can employ a very large high-frequency gain, which can significantly amplify high-frequency noise [28], [29] and provide an excessive enhancement some bright pixels – causing their intensities to be clipped the highest gray-level – thus resulting in a loss of image content [30]. Fig. 7 illustrates the effect of such an excessive high-frequency enhancement in a deblurring operation.

In order to demonstrate linear deblurring filters with constrained high-frequency gain, we have selected Wiener deconvolution and constrained least square restoration with smoothness constraint (hereon referred to as CLSR). The details of these filters can be found in digital image processing texts such as Castleman [28], and Gonzalez and Woods [29]. Both Wiener deconvolution and CLSR constrain their high-frequency gain based on an estimation of noise power from

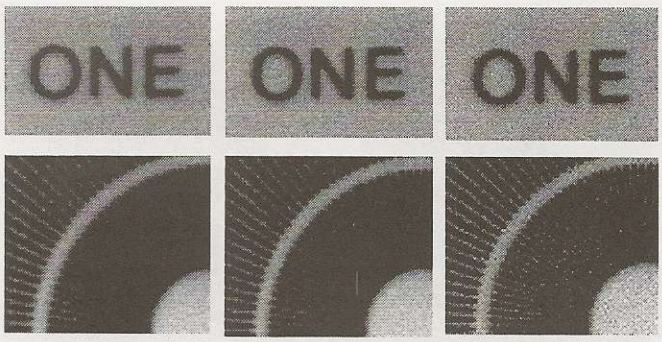

(a) (b) (c)

Fig. 2 An illustration of excessive high-frequency gain in a deblurring operation. (a) captured images from ZR32112, (b) inverse filtering, (c) a deblurring operation with excessive high-frequency gain.

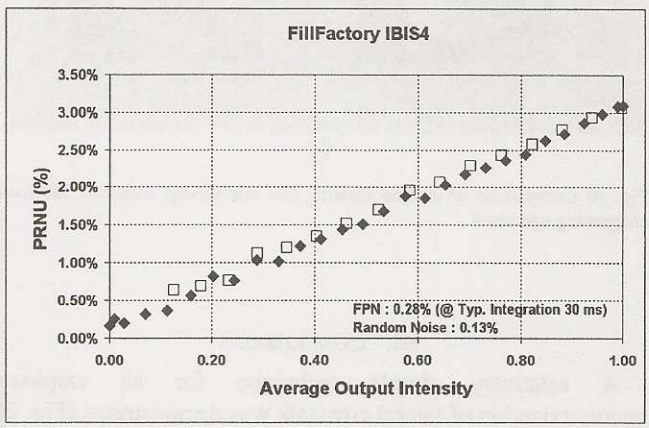

Fig. 3 Photoresponse non-uniformity (PRNU) measurements on IBIS4 and ZR32112 using monochromatic illumination source (λ = 540 nm) and an integrating sphere. The solid dots were obtained by varying integration time at constant illumination; the hollow dots were obtained by varying illumination intensity with a fixed integration time. Both fixed pattern noise (FPN) and random noise were measured in dark with integration time of 30 ms.

the input image. Given that we know the observed noise predominantly originates from the sensor itself, the noise estimation was extracted from the measured noise characteristic of the employed image sensors. Fig. 8 summarizes the noise measurements performed on IBIS4 and ZR32112. The photoresponse non-uniformity (PRNU) was measured at various illumination intensities and at various integration times (with frame averaging to remove random noise). The random noise was measured by subtracting the dark frame from each captured frame and averaging the noise power over one hundred frames.

In both sensors PRNU was significantly higher than the observed fixed pattern noise (FPN) and random noise. Fig. 8 illustrates that PRNU varies linearly with the average intensity of the output image and behaves essentially independent of both the incident illumination intensity and the integration time.[†] As the noise characteristics in both sensors were dominated by PRNU, the noise estimations in Wiener deconvolution and CLSR were obtained from the measured values of PRNU. The highest value of the measured PRNU was used for the noise power estimation, as the noise levels in the employed CMOS image sensors were found to be rather low for an illustrative demonstration of the noise adaptive filters.

Fig. 9 compares the results of inverse filtering, Wiener deconvolution, and CLSR on various captured images of IBIS4. Due to the low level of noise in IBIS4 (< 3.5%), the three filters produce comparable results. The constrained high-frequency gain in Wiener deconvolution and CLSR lead to a slightly compromised deblurring as indicated by MTF values calculated from the deblurred images. The amplification of high-frequency noise in Wiener deconvolution and CLSR is also slightly lower as expected. Other linear deblurring filters offer similar trade-offs between the image sharpness and the moderation of high-frequency amplification. A quantitative evaluation of various trade-offs can lead to a deblurring filter that is optimized for a given imaging system. In addition, in cases where a suitable compromise between the trade-offs cannot be achieved with linear deblurring operation, adaptive or non-linear methods can be considered further improve on the restoration.

The implementation of a deblurring operation can significantly vary depending on the final blur model of the system.[‡] As the ideal deblurring operation may be too costly to implement, a viable alternative may entail utilization of a sharpening filter devised with a trial-and-error method. Fig. 10 compares the results of inverse filtering, unsharp masking, and blur subtraction on the output images of IBIS4 [28], [29]. The result of blur subtraction demonstrates significant amount of high-frequency artifacts introduced by the sharpening filter. It can thus be appreciated that while a sharpening filter may be utilized to achieve similar effects as a restorative deblurring operation, a careful design is required in order to minimize the introduction of undesirable artifacts.

[†] This suggests that for both sensors, PRNU originates dominantly from the mismatches in readout (and amplifying) circuits rather than from the mismatches in photosensitive device (e.g. photodiode, photogate), which may lead to a more noticeable dependence on the incident illumination level or the integration time.

[‡] The design methods for linear and non-linear adaptive deblurring filters and their suitable implementations can be found in digital image processing and filter design texts [28], [29], [31], [32].

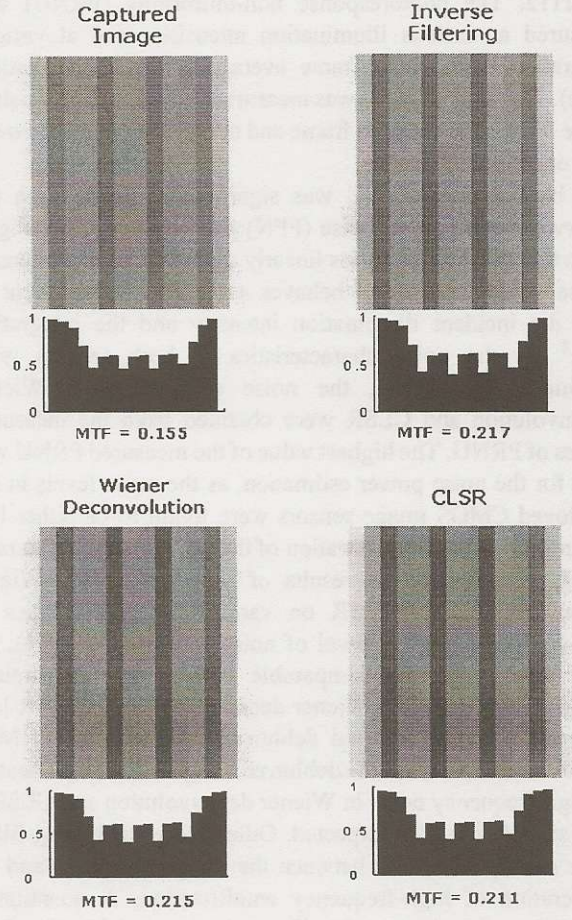

Fig. 4 Comparison of inverse filtering, Wiener deconvolution, and CLSR on a test image captured with IBIS4.

(a)

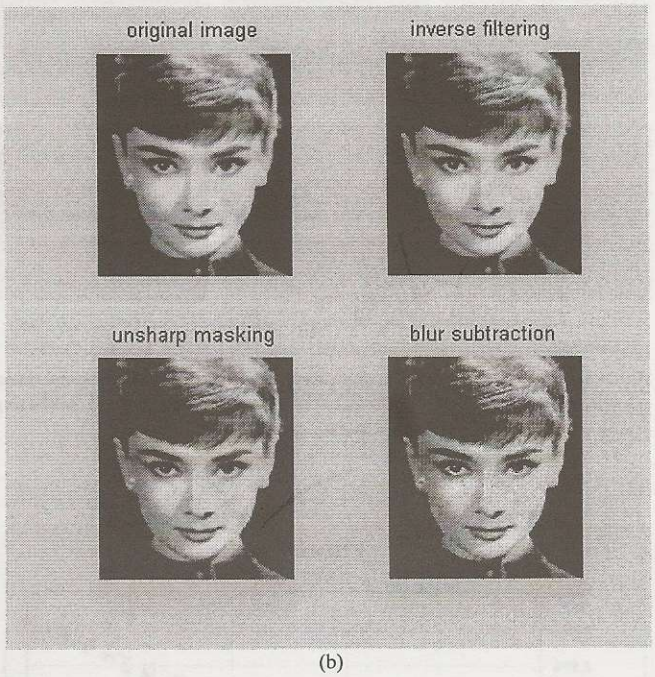

(b)

Fig. 50 Comparison of inverse filtering (i.e. deblurring) with two 3x3 local sharpening operators.

III. Conclusions

A relatively simple technique for an empirical characterization of lateral crosstalk was demonstrated (Fig. 2). The blurring effect of lateral crosstalk was characterized by the cross-responsivity PSF of an imaging array obtained from a single pixel excitation (Fig. 4) [22]. The inverse filter, Wiener deconvolution, and constrained least square restoration with smoothness constraint were used to demonstrate deblurring lateral crosstalk (Fig. 9). The noise estimation in Wiener deconvolution and CLSR was obtained from the measured PRNU of four CMOS image sensors as it dominated the noise characteristics in the employed sensors (Fig. 8). The comparison of linear deconvolution filters led to a brief illustration of the tradeoffs in image sharpness and the high-frequency noise effects.

Acknowledgment

The authors gratefully acknowledge the financial support from Canada's Network of Centers of Excellence and Natural Sciences and Engineering Research Council of Canada. The design support and fabrication services of Canadian Microelectronics Corporation are also gratefully acknowledged.

References

[1] S. K. Mendis, S. E. Kemeny, R. C. Gee, B. Pain, Q. Kim, and E. R. Fossum, "Progress in CMOS active pixel image sensors,"

Charge-Coupled Dev. And Solid State Opt. Sensors IV, Proc. SPIE. Vol. 2172, pp. 19-29, 1994

[2] O. Yadid-Pecht, "The geometrical modulation transfer function (MTF) – for different pixel active area shapes," *Optical Engineering*, vol. 39, no. 4, pp. 859-865, 2000

[3] I. Shcherback, and O. Yadid-Pecht, "CMOS APS MTF modeling," *IEEE Trans. on Electron Devices*, vol. 48, no. 12, pp. 2710-2715, 2001.

[4] C. Marques, and P. Magnan, "Experimental characterization and simulation of quantum efficiency and optical crosstalk of CMOS photodiode APS," *Electronic Imaging 2002, Conf. 4669A - Sensors, Cameras, and Systems for Scientific/Industrial Applications IV*, San Jose, CA, 2002.

[5] H. A. Maclead, *Thin-film Optical Filters*, Adam Hilger Ltd., 1986.

[6] X. Liu, P. Catrysse, and A. El Gamal, "QE reduction due to pixel vignetting in CMOS Image Sensors," *Proc. of the SPIE Electronic Imaging '2000 conference*, vol. 3965, San Jose, CA, 2000.

[7] P. B. Catrysse and B. A. Wandell, "Optical efficiency of image sensor pixels," *J. Opt. Soc. Am. A*, vol. 19, no. 8, pp. 1610-1620, 2002.

[8] J. Shappir, and A. Kolodny, "The Response of Small Photovoltaic Detectors to Uniform Radiation," *IEEE Trans. Electron Devices*, vol. ED-24, no. 8, pp. 1093-1097, August 1977.

[9] T. I. Kamins and G. T. Fong, "Photosensing arrays with improved spatial resolution," *IEEE Trans. Electron Devices*, vol. ED-25, no. 2, pp.154-159, February 1978.

[10] H. Holloway, "Theory of lateral-collection photodiodes," *J. Appl. Phys.*, vol. 49. no. 7, pp. 4264-4269, July 1978.

[11] S. Kirkpatrick, "Modeling Diffusion and Collection Charge from Ionizing Radiation in Silicon Devices," *IEEE Trans. Electron Devices*, vol. ED-26, pp. 1742-1753, November 1979.

[12] H. Holloway, and A.D. Brailsford, "Diffusion limited saturation current of a finite p-n junction," *J. Appl. Phys.*, vol. 55, no. 2, pp. 446-453, January 1984.

[13] A. D. Brailsford and H. Holloway, "Peripheral photoresponse of a large p-n junction in a thick semiconductor," *J. Appl. Phys.*, vol. 56, no. 4, pp. 1008-1011, August 1984.

[14] H. Holloway, and A.D. Brailsford, "Peripheral photoresponse of a p-n junction," *J. Appl. Phys.*, vol. 54, no. 8, pp. 4641-4656, August 1983.

[15] L. M. Sander, "Exact solution for the peripheral photoresponse of a p-n junction," *J. Appl. Phys.*, vol. 57, no. 6, pp. 2057-2059, March 1985.

[16] H. Holloway, "Collection efficiency and crosstalk in closely spaced photodiode arrays," *J. Appl. Phys.*, vol. 60, no. 3, pp. 1091-1096, August 1986.

[17] J. S. Lee, R. I. Hornsey, "Photoresponse of photodiode arrays for solid-state image sensors" J. Vacuum Science and Technology A, vol. 18, no. 2, pp. 621-625, 2000

[18] F. C. Ellot, "Geometric design of linear array detectors," I*EEE Trans. Electron Devices*, vol. ED-21, pp.613-616, October 1974.

[19] D. H. Seib, "Carrier diffusion degradation of modulation transfer function in charge coupled imagers," *IEEE Trans. Electron Devices*, vol. ED-21, pp. 210-217, March 1974.

[20] M. M. Blouke and D.A. Robinson, "A method for improving the spatial resolution of frontside-illuminated CCD's," *IEEE Trans. Electron Devices*, vol. ED-28, pp. 251-256, March 1981.

[21] J. P. Lavine, E. A. Trabka, B. C. Burkey, T. J. Tredwell, E. T. Nelson, and C. N. Anagnostopoulos, "Steady-state photocarrier collection in silicon imaging devices," *IEEE Trans. Electron Devices*, vol. ED-30, pp. 1392-1394, September 1983.

[22] D. Levy and S. E. Schacham, "Three-dimensional analytical simulation of self- and cross-responsivities of photovoltaic detector arrays," *IEEE Trans. Electron Devices*, vol. ED-34, no. 10, pp. 2059-2069, October 1987.

[23] D. Levy, S. E. Schacham, and I. Kidron, "Three-dimensional analytical model for photovoltaic detector arrays," IEDM, pp. 373-376, 1986.

[24] D. Levy, and S. E. Schacham, "Three-dimensional excess carrier distribution in semiconductor imaging arrays," J. Appl. Phys., vol. 64, no. 10, pp. 5230-5233, November 1988.

[25] J. S. Lee, R. I. Hornsey, and D. Renshaw, "Analysis of CMOS Photodiodes—Part I: Quantum Efficiency," *IEEE Trans. Electron Devices*, accepted for publication in May 2003.

[26] J. S. Lee, R. I. Hornsey, and D. Renshaw, "Analysis of CMOS Photodiodes—Part II: Lateral Photoresponse," *IEEE Trans. Electron Devices*, accepted for publication in May 2003.

[27] A. El Gamal, "Introduction to Image Sensors and Digital Cameras (Lecture notes)," Stanford University, CA, 2001.
Available: http://www.stanford.edu/class/ee392b

[28] K. G. Castleman, *Digital Image Processing*, Prentice Hall, 1996.

[29] R. C. Gonzalez and R. E. Woods, *Digital Image Processing*, Addison Wesley, 1992.

[30] H. Haneishi, R. Ohtake, N. Tsumura, Y. Miyake, P. C. Hung, H. Roehrig, and W. J. Dallas, "Sharpness matching between digital image display devices," *Optical Review*, vol. 5, no. 3, pp. 163-173, 1998.

[31] T.W. Parks and C.S. Burrus, *Digital Filter Design*, Wiley, New York, 1987

[32] J. G. Proakis and D.G. Manolakis, *Digital Signal Processing Principles, Algorithms, and Applications*, Prentice Hall, 2000.